Available online at www.sciencedirect.com
ScienceDirect
Journal of Sound and Vibration 309 (2008) 718–729
JOURNAL OF SOUND AND VIBRATION
www.elsevier.com/locate/jsvi

Exact spectral elements for follower tension buckling by power series

A.Y.T. Leung*

Department of Building and Construction, City University of Hong Kong, Hong Kong

Received 6 February 2007; received in revised form 22 June 2007; accepted 28 July 2007

Abstract

The spectral dynamic stiffness method using exact solutions of the governing equations as shape functions has been popular for vibration and dynamic stability analyses of framed structures consisting of uniform members. Since non-uniform members do not generally have closed form solutions, special cases only have been considered. However, exact solutions are still possible for generally non-uniform members using power series. The paper studies the exact dynamic stability of columns with distributed axial force by power series. Both uniform and distributed, compression and tension, and conservative and non-conservative axial forces are considered. Interaction diagrams of various kinds of axial loads on the natural frequencies including different intensities of the distributed loads and degree of tangency are given. Follower tension buckling is reported for the first time. It is found that the power series outperforms the dynamic stiffness method in terms of versatility in applications and numerical stability at the very low and high ends of the frequency spectrum.

1. Introduction

The spectral finite element method or the dynamic stiffness method has been widely used for structural response analysis [1–6]. Eisenberger [5] used power series to obtain the exact dynamics stiffness for non-uniform members. Lee and Park [7] performed spectral element analysis of a pipeline conveying internal unsteady fluid. Kim et al. [8] derived the exact dynamic stiffness matrix of non-symmetric thin-walled beams on elastic foundation using power series method. Finnveden [9,10], Langley [11] and Leung [12] investigated random vibration using spectral elements.

Langthjem and Sugiyama [13] and Elishakoff [14] reviewed the topic on follower forces which was studied extensively by Bolotin [15]. The aim of the present paper is to report on a new phenomenon of follower tension buckling which has not been mentioned in the previous references.

We shall use the exact spectral elements to study the dynamic stability of beam columns and structures under conservative and follower forces in this paper. The formulation of the exact spectral elements for beam columns is briefly discussed in Section 2 and exact solutions are given in Section 3. Interaction diagrams are compared with the exact dynamic stiffness method [4] whenever possible in Section 4. New results of follower

*Tel.: +852 27887600; fax: +852 27887612.
E-mail address: Andrew.leung@cityu.edu.hk

0022-460X/$ - see front matter © 2007 Elsevier Ltd. All rights reserved.
doi:10.1016/j.jsv.2007.07.058

tension are given and follower tension buckling under uniformly distributed follower tension is originally reported. The readers are referred to Langthjem and Sugiyama [13] and Elishakoff [14] for a comprehensive review of follower compression with more than 200 references in total. Effects of follower tension have not been reported in literatures.

2. Governing equations

The total potential energy for a beam-column subject to distributed tension axial force $P(x)$ and lateral force $f(x)$ per unit length at position x from the left end is

$$V = \frac{1}{2}\int [\mathrm{EI}(v'')^2 - P(v')^2 - 2fv]\,\mathrm{d}x, \tag{1}$$

where EI is the flexural rigidity and a dash denotes derivative with respect to x. In Eq. (1), the deflection v in the y direction is considered under the usual assumptions associated with thin beams. The stationary principle of total potential energy states that the variation of the total potential energy is zero when in equilibrium, Eq. (1) gives

$$\delta V = \mathrm{EI}\, v''\delta v'|_b - [(\mathrm{EI}\, v'')' - Pv']\delta v|_b + \int [(\mathrm{EI}\, v'')'' - (Pv')' - f]\delta v\,\mathrm{d}x = 0, \tag{2}$$

where $|_b$ denotes evaluation at the boundaries. Eq. (2) gives the governing equation

$$(\mathrm{EI}\, v'')'' - (Pv')' - f = 0 \tag{3}$$

and the boundary conditions:

$$\mathrm{EI}\, v''\,\delta v' - [(\mathrm{EI}\, v'')' - Pv']\delta v = 0, \quad \text{or} \quad M\,\delta v' + Q\,\delta v = 0 \tag{4}$$

in which the boundary shears and moments are, respectively,

$$Q = Pv' - (\mathrm{EI}\, v'')', \quad M = \mathrm{EI}\, v''. \tag{5}$$

For beam column on elastic foundation of modulus k, f should include the elastic reaction from the foundation $-kv$; and for vibration problem, f should include the inertia force $-\rho A\ddot{v}$ where dots denote differentiations with respect to time. The total mass is given by the product of mass density ρ, cross-sectional area A and length l of the beam column, respectively. For harmonic vibration with frequency ω, one can put $v(x,t) = v(x)\sin(\omega t)$ and the inertia force becomes

$$-\rho A\ddot{v}(x,t) = \rho A\omega^2 v(x)\sin(\omega t). \tag{6}$$

Substituting Eq. (6) into Eq. (2) and cancelling $\sin(\omega t)$, one has the governing equation for the amplitude of vibration $v(x)$:

$$(\mathrm{EI}\, v'')'' - (Pv')' - \omega^2\rho A v = 0 \tag{7}$$

and the associated boundary conditions (4) and (5). We use the same symbol for displacement and its amplitude when no confusion arises. For uniform beam columns, Eq. (7) can be non-dimensionalized to

$$v'''' - (pv')' - \lambda^4 v = 0, \tag{8}$$

where a dash denotes differentiation with respect to x/l. $p = P/\mathrm{EI}$ and $\lambda^4 = \omega^2\rho A l^4/\mathrm{EI}$ and the associated boundary conditions become

$$v''\,\delta v' - [v''' - pv']\delta v = M\,\delta v' + V\,\delta v = 0. \tag{9}$$

3. Solution by power series

Assuming, without loss of generality,

$$p(x) = p_1 + p_2 x + p_3 x^2 \tag{10}$$

and the solution of Eq. (8) with coefficients v_j to be determined,

$$v(x) = \sum_{j=1}^{n} v_j x^{j-1}, \tag{11}$$

one has, after substituting into Eq. (8) and comparing similar terms of x^j,

$$v_{5+j} = \frac{[\lambda^4 + jp_3(1+j)]v_{1+j} + (1+j)^2 p_2 v_{2+j} + (1+j)(2+j)p_1 v_{3+j}}{(1+j)(j+2)(j+3)(j+4)}. \tag{12}$$

Since there are four discrete boundary conditions, two at each of the two ends, the displacement function (11) can be expressed in terms of the integration constants v_1, v_2, v_3, v_4 as shown in Appendix A when $n = 15$ so that

$$v(x) = \sum_{j=1}^{n} v_j x^{j-1} = [\,\chi_1(x) \quad \chi_2(x) \quad \chi_3(x) \quad \chi_4(x)\,] \begin{Bmatrix} v_1 \\ v_2 \\ v_3 \\ v_4 \end{Bmatrix} = \boldsymbol{\chi}(x)\mathbf{r}, \tag{13}$$

$$\boldsymbol{\chi}(x) = \begin{bmatrix} \chi_1(x) & \chi_2(x) & \chi_3(x) & \chi_4(x) \end{bmatrix} \text{ and } \mathbf{r} = \begin{Bmatrix} v_1 \\ v_2 \\ v_3 \\ v_4 \end{Bmatrix}.$$

It is also observed that the coefficients decay like $n!$ and therefore the displacement function always converges rapidly for any combination of p and λ. To achieve machine precision of 10^{-14}, one must set $\lambda^n/n! < 10^{-14}$. The Stirling formula states that $n! \approx \sqrt{2\pi n} n^n \mathrm{e}^{-n}$ for large n. Therefore, one can estimate the number of terms for a particular value of frequency parameter to achieve the required precision.

To get the shape function from the displacement function (13), the following displacement boundary conditions are required:

$$\boldsymbol{\delta} = \begin{Bmatrix} v(0) \\ v'(0) \\ v(1) \\ v'(1) \end{Bmatrix} = \begin{bmatrix} \boldsymbol{\chi}(0) \\ \boldsymbol{\chi}'(0) \\ \boldsymbol{\chi}(1) \\ \boldsymbol{\chi}'(1) \end{bmatrix} \mathbf{r} = \mathbf{C}\mathbf{r} \text{ for } \mathbf{C} = \begin{bmatrix} \boldsymbol{\chi}(0) \\ \boldsymbol{\chi}'(0) \\ \boldsymbol{\chi}(1) \\ \boldsymbol{\chi}'(1) \end{bmatrix} \text{ or } \mathbf{r} = \mathbf{C}^{-1}\boldsymbol{\delta} \text{ and} \tag{14}$$

$$v(x) = \boldsymbol{\chi}(x)\mathbf{r} = \boldsymbol{\chi}(x)\mathbf{C}^{-1}\boldsymbol{\delta} = \mathbf{N}(x)\boldsymbol{\delta}, \tag{15}$$

where $\mathbf{N}(x) = \boldsymbol{\chi}(x)\mathbf{C}^{-1}$ is the shape function matrix in finite element sense. The dynamic stiffness matrix $\mathbf{D}$ is given by

$$\mathbf{F} = \begin{Bmatrix} -V(0) \\ -M(0) \\ V(1) \\ M(1) \end{Bmatrix} = \mathbf{D}\boldsymbol{\delta}. \tag{16}$$

Due to the reciprocal theorem, the dynamic stiffness matrix must be symmetrical when the loading is conservative. The paper considers both conservative and non-conservative loads and their combination as shown in Fig. 1.

The boundary forces and moments for the conservative case are the same as given by Eq. (9), i.e.,

$$M = v'' \text{ and } V = pv' - v'''. \tag{17}$$

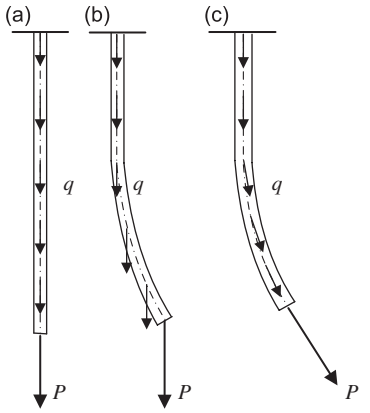

Fig. 1. Columns subject to uniform axial or follower forces.

If the axial loads are follower, then

$$M = v'' \text{ and } V = -v'''. \tag{18}$$

If the axial loads are partially follower of fraction m, which is called the degree of tangency, then

$$M = v'' \text{ and } V = (1-m)pv' - v'''. \tag{19}$$

when p is constant, analytical solutions in terms of exponential functions are readily available [4].

4. Numerical examples

Numerical examples of buckling problems of columns subjected to conservative or follower tension and are considered in this study. The relationships of

$$\lambda = \left(\frac{\rho A l^4 \omega^2}{\mathrm{EI}}\right)^{1/4}, \quad \sigma_p = \left(\frac{pl^2}{\mathrm{EI}}\right)^{1/2} \text{ and } \sigma_q = \left(\frac{pql^3}{\mathrm{EI}}\right)^{1/2},$$

where the distributed axial load is given by $p(1+qx)$ are shown in the subsections below.

4.1. Conservative buckling problems of columns

Analytical dynamic stiffness and substructure method has been used by Leung [4] to solve the buckling problems of columns subject to uniformly distributed axial forces. In this section the results calculated by power series will be compared with Leung's results. The influence of axial compression on the natural frequency is given in Fig. 2 showing the lowest two modes. The zigzag line in Fig. 2 corresponds to the pole line where the dynamic stiffness is positive infinity on one side and negative infinity on the other side. The pole line can be removed by dividing the dynamic stiffness by det$\mathbf{C}$. The pole lines of the subsequent interaction diagrams are eliminated using the technique.

The interaction diagram for a cantilever column subject to axial tension is compared with the analytic dynamic stiffness matrix method in Fig. 3, in which the narrow full lines are the results from the exact dynamic stiffness method and the thick dashed lines from the power series. No difference can practically be found. It is shown that the power series is numerically stable even for very high modes while the exact dynamic stiffness method is numerically unstable due to the cancellation of large numbers in both the numerator and the denominator of the frequency functions in the non-symmetric dynamic stiffness resulting in some blurred areas in the diagrams.

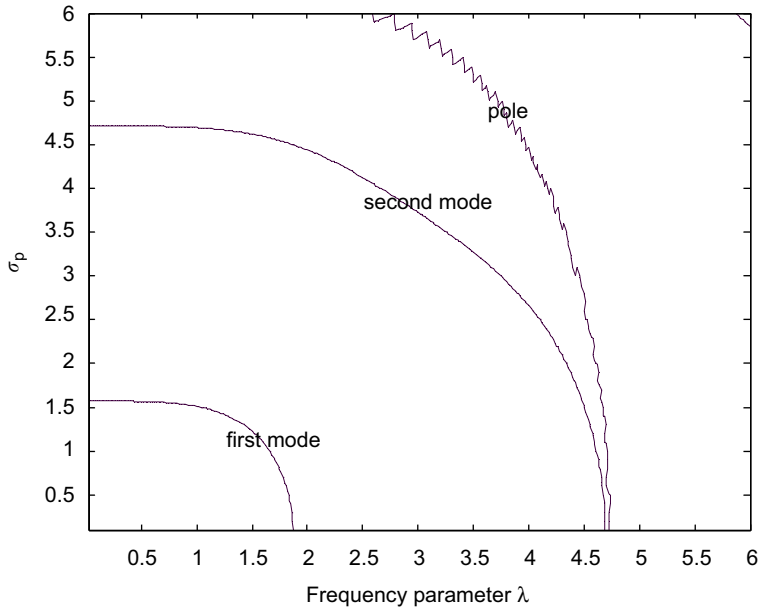

Fig. 2. Influence of compressive force on the natural frequency.

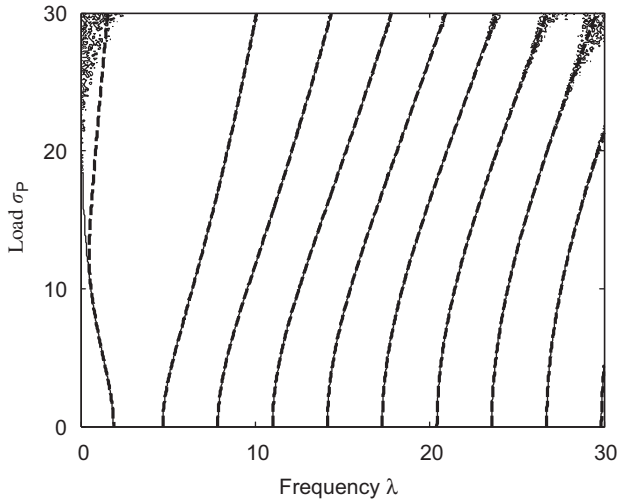

Fig. 3. Clamped–free column subject to uniform follower tension.

4.2. *Buckling problems of columns under axial tension and follower tension*

Consider a beam-column subject to uniform follower tension or distributed follower tension. The interaction diagram for a cantilever column is compared with the column subject to conservative uniform tension in Fig. 4a–d and conservative distributed tension in Fig. 5a–d for various boundary conditions. The narrow full lines and the thick dashed lines are the results for the column subject to follower tension and conservative tension, respectively. Only one element is used in all cases.

4.2.1. *Uniform axial tension*

There is no difference for all boundary conditions when subject to uniform follower axial tension or conservative axial tension except for clamped–free condition as shown in Figs. 4a–d. The phenomenon that

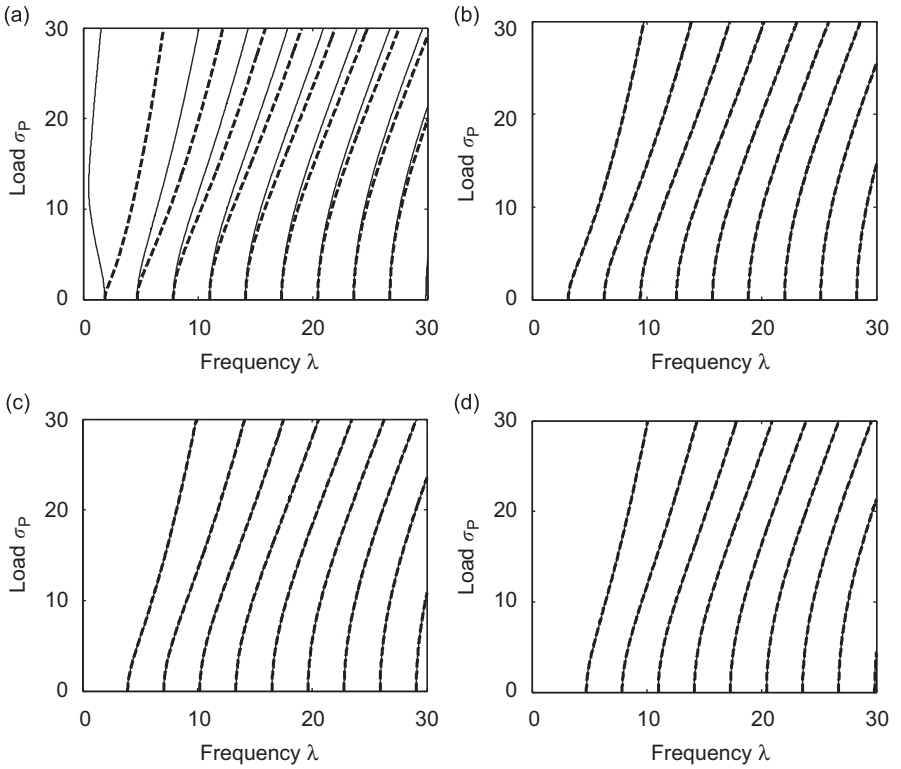

Fig. 4. (a) Clamped–free column subject to uniform tension, (b) hinged–hinged column subject to uniform tension, (c) clamped–hinged column subject to uniform tension and (d) clamped–clamped column subject to uniform tension.

the first mode has negative gradient in the interaction diagram only happens to the clamped–free condition subject to follower tension. The same phenomenon is checked as correct by the analytic dynamics stiffness method. In the figures, dotted lines are for conservative loads and solid lines are for follower forces.

4.2.2. Distributed loads

Similarly, there is no much difference for all boundary conditions when subject to distributed follower axial tension or conservative axial tension except for clamped–free condition as shown in Figs. 5a–d. The phenomenon that the first mode has negative gradient in the interaction diagram only happens to the clamped–free condition subject to follower tension. The same phenomenon cannot be checked by the analytic dynamics stiffness method which works for uniform axial loads only. In the figures, dotted lines are for conservative loads and solid lines are for follower forces.

4.3. Interaction diagrams with various distributed loads

The influence of the distributed axial force $\sigma^2 = p(1+qx)$ on the natural frequency $\lambda^4 = \omega^2\rho Al/\mathrm{EI}$ is studied here. The parameter p has the unit of force (Newton) and the parameter q has the unit of reciprocal of length (m^{-1}) representing the strength of linearly distributed force. Figs. 6a and b show the conservative and follower interaction diagrams respectively when the axial forces are compressive, while Figs. 7a and b give the corresponding diagrams for tension axial forces.

The interaction lines in Fig. 6a do not have inflexion points and flutter loads are obviously observed in Fig. 6b. The interaction lines in Fig. 7a always have inflexion points for conservative tension. The inflexion curve is much magnified for follower tension when $q = 0$. When q is non-zero, follower tension buckling is possible. The phenomenon is reported here for the first time.

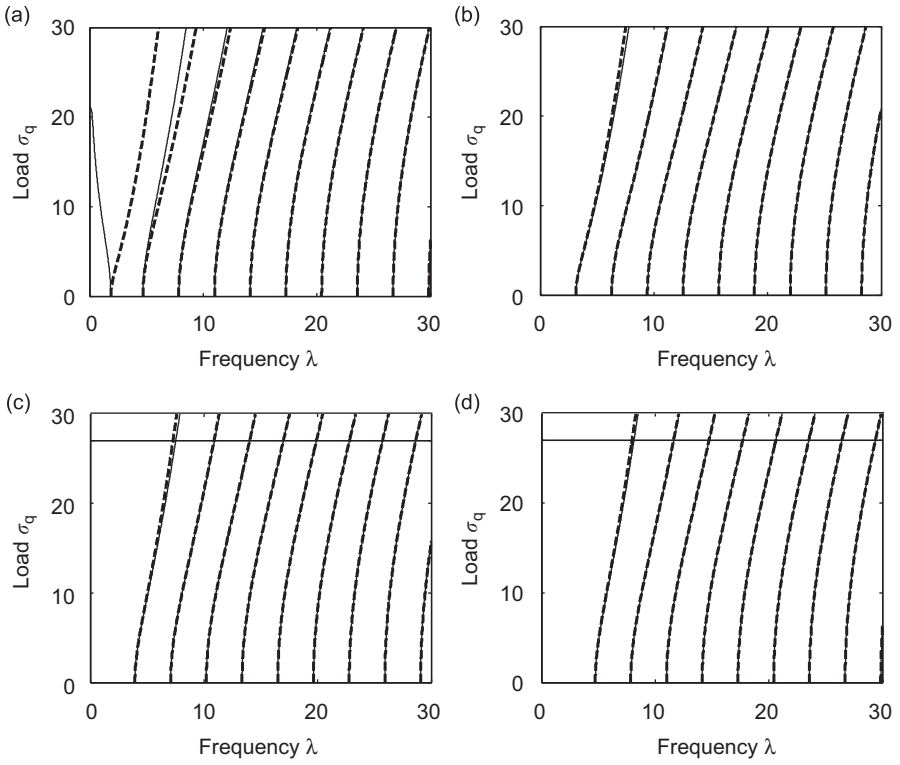

Fig. 5. (a) Clamped–free column subject to distributed tension, (b) hinged–hinged column subject to distributed tension, (c) clamped–hinged column subject to distributed tension and (d) clamped–clamped column subject to distributed tension.

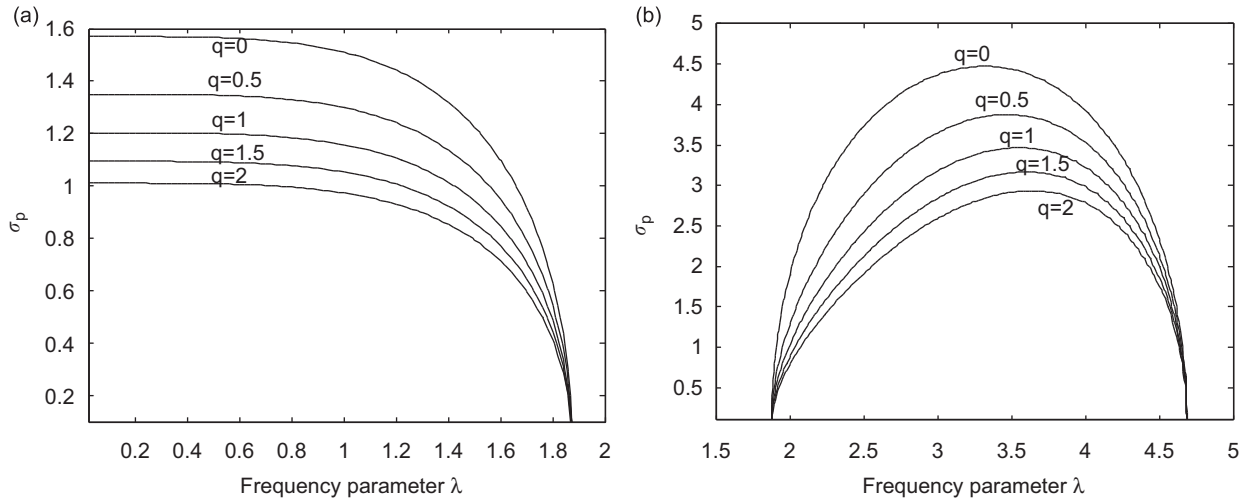

Fig. 6. (a) Influence of q on the interaction diagram, conservative compressive and (b) influence of q on the interaction diagram, follower compressive.

4.4. Interaction diagrams for partially follower force

Define the degree of tangency m in Eq. (19) as the fraction of the uniform follower compressive load. One has the interaction diagram for the first two modes in Fig. 8. It is interesting to note that most curves pass through the point $(\lambda, \sigma_p) = (2.667,4.00)$. It is just a coincidence without important physical meaning.

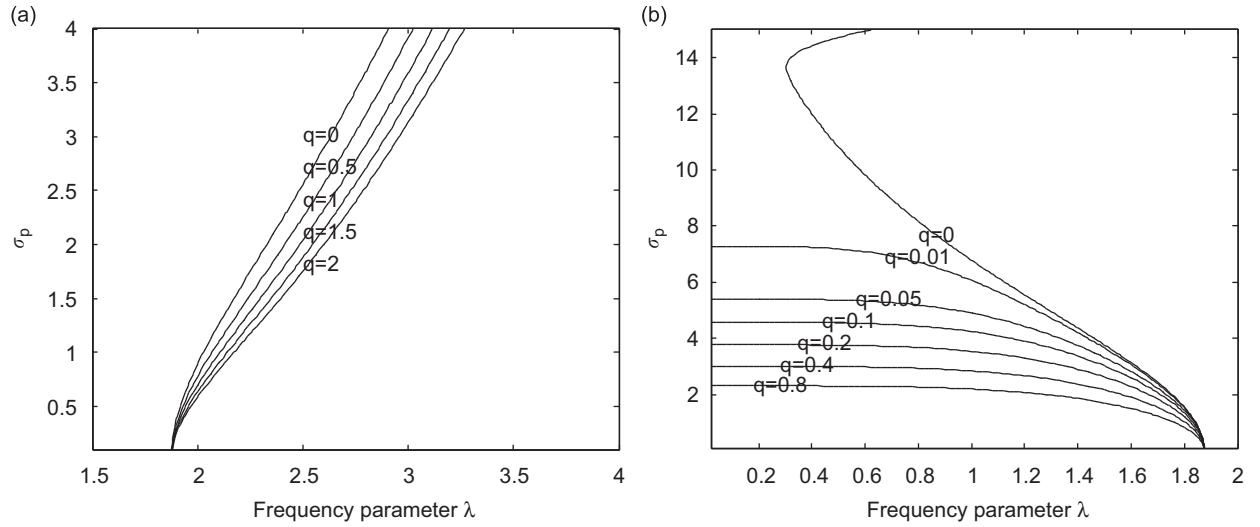

Fig. 7. (a) Influence of q on the interaction diagram, conservative tension and (b) influence of q on the interaction diagram, follower tension.

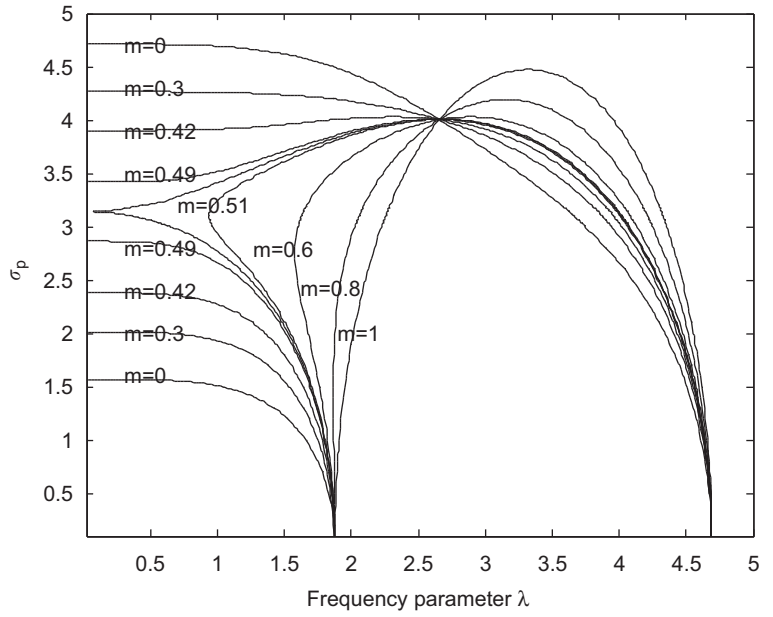

Fig. 8. The influence of tangency on the interaction diagram.

The line for $m = 0.5$ is unmarked. When $m<0.5$, coalescence of two modes is not possible but flutter can still be observed. For example, when $m = 0.49$, the curve moves up from $\lambda = 0$ and reaches maximum at $(\lambda,\sigma_p) = (2.85,4.03)$. Slight increase from $\sigma_p = 4.03$ will result in a pair of complex natural frequencies represent classical flutter.

4.5. Influence of end mass

Consider the influence of a concentrated mass M as shown in Fig. 9, such that $M = r\rho Al$ for various values of r. When the mass is attached on the free end of the column, the modification of the mass matrix is to include

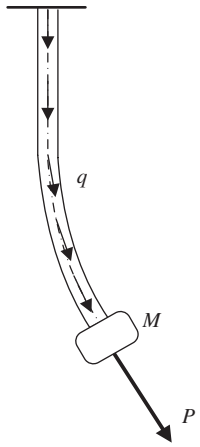

Fig. 9. Follower axial tension with an end mass.

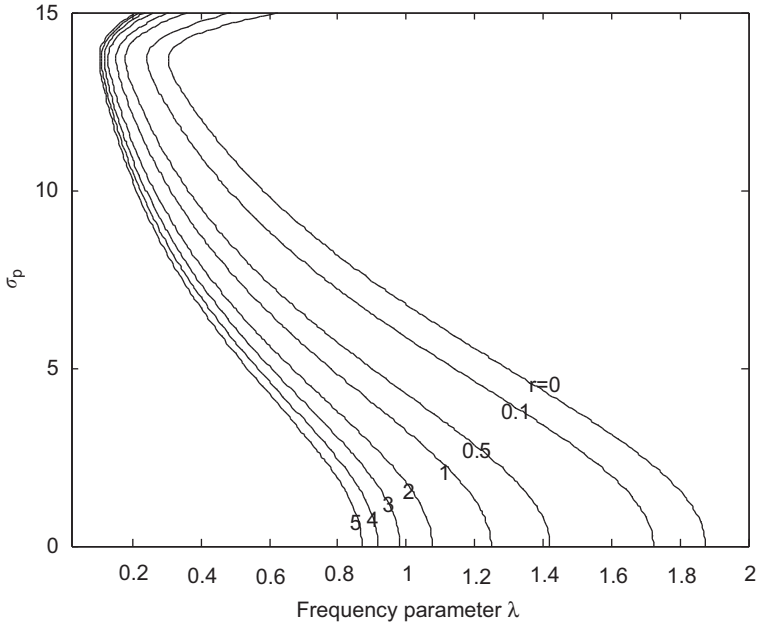

Fig. 10. The influence of mass ratio r on the first mode.

the term $\mathbf{M}^e(3,3) = M$ at the entry $(3, 3)$ of the mass matrix. When the columns are subject to uniform follower axial tension, the interaction diagram is given in Fig. 10. It is found that the end mass has significant influence on the natural modes of column quantitatively but not qualitatively.

5. Discussion and conclusion

Follower tension buckling was mentioned without results by Zyczkowski in Ref. [16, p. 273] using an example of a vessel loaded by a liquid shown in Fig. 11 which was investigated by Gajewski and Palej (1974). Unfortunately, the author could not find such reference. Therefore, it may be concluded that follower tension buckling is originally reported at least in the western world. The exact spectral dynamic stiffness is very efficient in studying such problems.

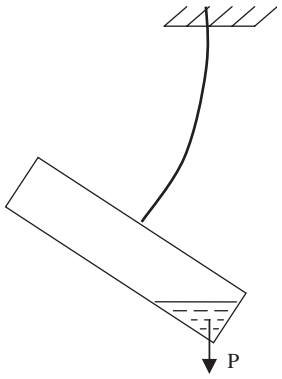

Fig. 11. A vessel loaded by a liquid.

Acknowledgement

The research is supported by the University Grant Council of Hong Kong Grant No. CityU 1157/06E.

Appendix A. Shape functions when $n = 15$ and $w = \lambda^4$

$$
\begin{aligned}
&v(x)\\
&= v_1\left(1+\frac{wx^4}{24}+\frac{1}{720}p_1wx^6+\frac{p_2wx^7}{1260}+\frac{p_1^2wx^8}{40320}+\frac{p_3wx^8}{2016}+\frac{w^2x^8}{40320}\right.\\
&\quad+\frac{p_1p_2wx^9}{36288}+\frac{p_1^3wx^{10}}{3628800}+\frac{p_2^2wx^{10}}{129600}+\frac{31p_1p_3wx^{10}}{1814400}+\frac{p_1w^2x^{10}}{1814400}+\\
&\quad+\frac{p_1^2p_2wx^{11}}{2217600}+\frac{p_2p_3wx^{11}}{103950}+\frac{p_2w^2x^{11}}{3326400}+\frac{p_1^4wx^{12}}{479001600}+\frac{59p_1p_2^2wx^{12}}{239500800}\\
&\quad+\frac{67p_1^2p_3wx^{12}}{239500800}+\frac{p_3^2wx^{12}}{332640}+\frac{p_1^2w^2x^{12}}{159667200}+\frac{23p_3w^2x^{12}}{119750400}+\frac{w^3x^{12}}{479001600}\\
&\quad+\frac{p_1^3p_2wx^{13}}{222393600}+\frac{p_2^3wx^{13}}{22239360}+\frac{17p_1p_2p_3wx^{13}}{55598400}+\frac{p_1p_2w^2x^{13}}{148262400}\\
&\quad+\frac{p_1^5wx^{14}}{87178291200}+\frac{79p_1^2p_2^2wx^{14}}{21794572800}+\frac{61p_1^3p_3wx^{14}}{21794572800}+\frac{83p_2^2p_3wx^{14}}{990662400}\\
&\quad+\frac{59p_1p_3^2wx^{14}}{622702080}+\frac{p_1^3w^2x^{14}}{21794572800}+\frac{p_2^2w^2x^{14}}{544864320}+\frac{17p_1p_3w^2x^{14}}{3962649600}\\
&\quad\left.+\frac{p_1w^3x^{14}}{29059430400}\right),
\end{aligned}
$$

$$
\begin{aligned}
&+v_2\left(x+\frac{p_2x^4}{24}+\frac{p_3x^5}{60}+\frac{wx^5}{120}+\frac{1}{720}p_1p_2x^6+\frac{p_2^2x^7}{1260}+\frac{p_1p_3x^7}{2520}\right.\\
&+\frac{p_1wx^7}{5040}+\frac{p_1^2p_2x^8}{40320}+\frac{p_2p_3x^8}{1344}+\frac{p_2wx^8}{6720}+\frac{p_1p_2^2x^9}{36288}+\frac{p_1^2p_3x^9}{181440}\\
&+\frac{p_3^2x^9}{6048}+\frac{p_1^2wx^9}{362880}+\frac{p_3wx^9}{11340}+\frac{w^2x^9}{362880}+\frac{p_1^3p_2x^{10}}{3628800}+\frac{p_2^3x^{10}}{129600}\\
&\left.+\frac{43p_1p_2p_3x^{10}}{1814400}+\frac{p_1p_2wx^{10}}{259200}+\frac{p_1^2p_2^2x^{11}}{2217600}+\frac{p_1^3p_3x^{11}}{19958400}\right.
\end{aligned}
$$

$$+\frac{29p_2^2p_3x^{11}}{2494800}+\frac{43p_1p_3^2x^{11}}{9979200}+\frac{p_1^3wx^{11}}{39916800}+\frac{13p_2^2wx^{11}}{9979200}+\frac{p_1p_3wx^{11}}{443520}$$
$$+\frac{p_1w^2x^{11}}{19958400}+\frac{p_1^4p_2x^{12}}{479001600}+\frac{59p_1p_2^3x^{12}}{239500800}+\frac{p_1^2p_2p_3x^{12}}{2721600}+\frac{p_2p_3^2x^{12}}{177408}$$
$$+\frac{p_1^2p_2wx^{12}}{19958400}+\frac{5p_2p_3wx^{12}}{3193344}+\frac{p_2w^2x^{12}}{319334400}+\frac{p_1^3p_2^2x^{13}}{222393600}+\frac{p_2^4x^{13}}{22239360}$$
$$+\frac{p_1^4p_3x^{13}}{3113510400}+\frac{139p_1p_2^2p_3x^{13}}{389188800}+\frac{p_1^2p_3^2x^{13}}{17690400}+\frac{p_3^3x^{13}}{1153152}$$
$$+\frac{p_1^4wx^{13}}{6227020800}+\frac{101p_1p_2^2wx^{13}}{3113510400}+\frac{p_1^2p_3wx^{13}}{34214400}+\frac{7p_2^2wx^{13}}{14826240}$$
$$+\frac{p_1^2w^2x^{13}}{2075673600}+\frac{61p_3w^2x^{13}}{3113510400}+\frac{w^3x^{13}}{6227020800}+\frac{p_1^5p_2x^{14}}{87178291200}$$
$$+\frac{79p_1^2p_2^3x^{14}}{21794572800}+\frac{p_1^3p_2p_3x^{14}}{283046400}+\frac{31p_2^3p_3x^{14}}{330220800}+\frac{1171p_1p_2p_3^2x^{14}}{7264857600}$$
$$+\frac{p_1^3p_2wx^{14}}{2421619200}+\frac{p_2^3wx^{14}}{145297152}+\frac{17p_1p_2p_3wx^{14}}{440294400}+\frac{17p_1p_2w^2x^{14}}{29059430400}\Bigg),$$

$$v_3\Bigg(x^2+\frac{p_1x^4}{12}+\frac{p_2x^5}{30}+\frac{p_1^2x^6}{360}+\frac{p^3x^6}{60}+\frac{wx^6}{360}+\frac{1}{420}p_1p_2x^7+\frac{p_1^3x^8}{20160}$$
$$+\frac{p_2^2x^8}{2016}+\frac{13p_1p_3x^8}{10080}+\frac{p_1wx^8}{10080}+\frac{p_1^2p_2x^9}{15120}+\frac{p_2p_3x^9}{1890}+\frac{p_2wx^9}{22680}$$
$$+\frac{p_1^4x^{10}}{1814400}+\frac{13p_1p_2^2x^{10}}{453600}+\frac{17p_1^2p_3x^{10}}{453600}+\frac{p_3^2x^{10}}{7200}+\frac{p_1^2wx^{10}}{604800}$$
$$+\frac{p_3wx^{10}}{37800}+\frac{w^2x^{10}}{1814400}+\frac{p_1^3p_2x^{11}}{997920}+\frac{p_2^3x^{11}}{249480}+\frac{p_1p_2p_3x^{11}}{31185}$$
$$+\frac{p_1p_2wx^{11}}{665280}+\frac{p_1^5x^{12}}{239500800}+\frac{p_1^2p_2^2x^{12}}{1496880}+\frac{p_1^3p_3x^{12}}{1710720}+\frac{p_2^2p_3x^{12}}{151200}$$
$$+\frac{59p_1p_3^2x^{12}}{6652800}+\frac{p_1^3wx^{12}}{59875200}+\frac{41p_2^2wx^{12}}{119750400}+\frac{109p_1p_3wx^{12}}{119750400}$$
$$+\frac{p_1w^2x^{12}}{79833600}+\frac{p_1^4p_2x^{13}}{103783680}+\frac{p_1p_2^3x^{13}}{5189184}+\frac{p_1^2p_2p_3x^{13}}{1297296}+\frac{31p_2p_3^2x^{13}}{8648640}$$
$$+\frac{p_1^2p_2wx^{13}}{43243200}+\frac{p_2p_3wx^{13}}{2402400}+\frac{p_2w^2x^{13}}{172972800}+\frac{p_1^6x^{14}}{43589145600}$$
$$+\frac{19p_1^3p_2^2x^{14}}{2179457280}+\frac{p_2^4x^{14}}{49533120}+\frac{5p_1^4p_3x^{14}}{871782912}+\frac{163p_1p_2^2p_3x^{14}}{495331200}$$
$$+\frac{49p_1^2p_3^2x^{14}}{222393600}+\frac{p_3^3x^{14}}{1572480}+\frac{p_1^4wx^{14}}{8717829120}+\frac{29p_1p_2^2wx^{14}}{2724321600}$$
$$+\frac{p_1^2p_3wx^{14}}{70761600}+\frac{461p_3^2wx^{14}}{3632428800}+\frac{p_1^2w^2x^{14}}{7264857600}+\frac{79p_3w^2x^{14}}{21794572800}+\frac{w^3x^{14}}{43589145600}\Bigg),$$

$$+v_4\Bigg(x^3+\frac{p_1x^5}{20}+\frac{p_2x^6}{40}+\frac{p_1^2x^7}{840}+\frac{p_3x^7}{70}+\frac{wx^7}{840}+\frac{1}{840}p_1p_2x^8+\frac{p_1^3x^9}{60480}$$
$$+\frac{p_2^2x^9}{3360}+\frac{p_1p_3x^9}{1440}+\frac{p_1wx^9}{30240}+\frac{p_1^2p_2x^{10}}{40320}+\frac{p_2p_3x^{10}}{2880}+\frac{p_2wx^{10}}{60480}$$
$$+\frac{p_1^4x^{11}}{6652800}+\frac{41p_1p_2^2x^{11}}{3326400}+\frac{7p_1^2p_3x^{11}}{475200}+\frac{p_3^2x^{11}}{9900}+\frac{p_1^2wx^{11}}{2217600}$$

$$+\frac{17p_3wx^{11}}{1663200}+\frac{w^2x^{11}}{6652800}+\frac{p_1^3p_2x^{12}}{3326400}+\frac{p_2^3x^{12}}{492800}+\frac{97p_1p_2p_3x^{12}}{6652800}$$
$$+\frac{p_1p_2wx^{12}}{2217600}+\frac{p_1^5x^{13}}{1037836800}+\frac{29p_1^2p_2^2x^{13}}{129729600}+\frac{47p_1^3p_3x^{13}}{259459200}$$
$$+\frac{31p_2^2p_3x^{13}}{8648640}+\frac{53p_1p_3^2x^{13}}{12355200}+\frac{p_1^3wx^{13}}{259459200}+\frac{59p_2^2wx^{13}}{518918400}$$
$$+\frac{29p_1p_3wx^{13}}{103783680}+\frac{p_1w^2x^{13}}{345945600}+\frac{p_1^4p_2x^{14}}{415134720}+\frac{19p_1p_2^3x^{14}}{259459200}$$
$$+\frac{139p_1^2p_2p_3x^{14}}{518918400}+\frac{11p_2p_3^2x^{14}}{5241600}+\frac{p_1^2p_2wx^{14}}{172972800}+\frac{7p_2p_3wx^{14}}{49420800}+\frac{p_2w^2x^{14}}{691891200}\Bigg).$$

References

[1] S. Finnveden, Exact spectral finite element analysis of stationary vibrations in a rail way car structure, *Acta Acustica* 2 (1994) 461–482.

[2] S. Finnveden, Spectral finite element analysis of the vibration of straight fluid-filled pipes with flanges, *Journal of Sound and Vibration* 199 (1997) 125–154.

[3] R.S. Langley, Application of the dynamic stiffness method to the free and forced vibration of aircraft panels, *Journal of Sound and Vibration* 135 (1989) 319–331.

[4] A.Y.T. Leung, *Dynamic Stiffness and Substructures*, Springer, London, 1993.

[5] M. Eisenberger, Exact static and dynamic stiffness matrices for general variable cross-section members, *AIAA Journal* 28 (6) (1990) 1105–1109.

[6] E. Efraim, M. Eisenberger, Exact vibration frequencies of segmented axisymmetric shells, *Thin-Walled Structures* 44 (3) (2006) 281–289.

[7] U. Lee, J. Park, Spectral element modelling and analysis of a pipeline conveying internal unsteady fluid, *Journal of Fluids and Structures* 22 (2) (2006) 273–292.

[8] N.I. Kim, J.H. Lee, M.Y. Kim, Exact dynamic stiffness matrix of non-symmetric thin-walled beams on elastic foundation using power series method, *Advances in Engineering Software* 36 (8) (2005) 518–532.

[9] S. Finnveden, Exact spectral finite element analysis of stationary vibrations in a rail way car structure, *Acta Acustica* 2 (1994) 461–482.

[10] S. Finnveden, Spectral finite element analysis of the vibration of straight fluid-filled pipes with flanges, *Journal of Sound and Vibration* 199 (1997) 125–154.

[11] R.S. Langley, Application of the dynamic stiffness method to the free and forced vibration of aircraft panels, *Journal of Sound and Vibration* 135 (1989) 319–331.

[12] A.Y.T. Leung, Dynamic stiffness for structures with distributed deterministic or random loads, *Journal of Sound and Vibration* 242 (3) (2001) 377–395.

[13] M.A. Langthjem, Y. Sugiyama, Dynamic stability of columns subjected to follower loads: a survey, *Journal of Sound and Vibration* 238 (5) (2000) 809–851.

[14] I. Elishakoff, Controversy associated with the so-called 'follower forces': critical overview, *Applied Mechanics Reviews* 58 (2005) 117–142.

[15] V.V. Bolotin, *Non-Conservative Problems of the Theory of Elastic Stability*, Pergamon Press, Oxford, 1963.

[16] M. Zyczkowski, *Strength of Structural Elements*, Elsevier, Amsterdam, 1991.